Eur. Phys. J. B **47**, 231–237 (2005)
DOI: 10.1140/epjb/e2005-00322-1

THE EUROPEAN PHYSICAL JOURNAL B

Doping dependence of the vortex glass and sublimation transitions in the high–T_c superconductor $La_{2-x}Sr_xCuO_4$ as determined from macroscopic measurements

R. Gilardi[1,a], S. Streule[1], N. Momono[2], M. Oda[2], and J. Mesot[1]

[1] Laboratory for Neutron Scattering, ETH Zurich and PSI Villigen, 5232 Villigen PSI, Switzerland
[2] Departement of Physics, Hokkaido University, Sapporo 060-0810, Japan

Received 3 April 2005 / Received in final form 25 July 2005
Published online 11 October 2005 –

Abstract. Magnetization and ac-susceptibility measurements are used to characterize the mixed phase of the high-temperature cuprate superconductor $La_{2-x}Sr_xCuO_4$ over a large range of doping ($0.075 \leq x \leq 0.20$). The first order vortex lattice phase transition line $H_{FOT}(T)$, the upper critical field $H_{c2}(T)$ and the second peak $H_{sp}(T)$ have been investigated up to high magnetic fields (8 Tesla applied perpendicular to the CuO_2 planes). Our results reveal a strong doping dependence of the magnetic phase diagram, which can mainly be explained by the increasing anisotropy with underdoping. Within our interpretation, the first order vortex lattice phase transition is due to the sublimation (rather than melting) of the vortex lattice into a gas of pancake vortices, whereas the second peak is related to the transition to a more disordered vortex glass state.

PACS. 74.25.Ha Magnetic properties – 74.25.Qt Vortex lattices, flux pinning, flux creep – 74.72.Dn La-based cuprates

1 Introduction

Despite belonging to the family of the first high-T_c superconductor (HTSC) to be discovered, the magnetic phase diagram of $La_{2-x}Sr_xCuO_4$ (LSCO) has not been as intensively investigated as that of other cuprates such as $YBa_2Cu_3O_x$ (YBCO) and $Bi_2Sr_2CaCu_2O_{8+x}$ (BSCCO). The LSCO compound has a relative small value of T_c (38.5 K at optimal doping), but is of high interest because it fills the gap between rather 3D systems such as YBCO and highly anisotropic 2D systems such as BSCCO. The anisotropy factor γ^2 can be defined as the ratio between the out-of-plane and the in-plane resistive components (ρ_c/ρ_{ab}) measured in the normal state [1,2]. An additional advantage of LSCO is that γ depends on the Sr content x and allows a study of the magnetic phase diagram over a wide range of anisotropy ($200 < \gamma^2 < 4000$) which lies inbetween the values for YBCO ($25 < \gamma^2 < 100$) and BSCCO ($3000 < \gamma^2 < 30000$).

The magnetic phase diagram of HTSC cuprates is dominated by the mixed phase (the lower critical field $H_{c1}(0\ \mathrm{K})$ is about 10^{-2} T whereas the upper critical field $H_{c2}(0\ \mathrm{K})$ is of the order of 10^2 T), where the magnetic flux can penetrate into the sample in the form of quantized flux-lines (vortices). Due to the anisotropy and thermal fluctuations one observes a number of vortex phases, which have been the subject of extended experimental and theoretical research in the last two decades [3]. In LSCO one can distinguish between a first order transition (FOT) line $H_{FOT}(T)$, which has been attributed to the melting [3–5] or sublimation [1,2] of the vortex lattice into a vortex fluid, and the irreversibility line $H_{irr}(T)$, where reversible magnetization and resistivity appear [1,2,6]. Another interesting feature is the so-called *fishtail effect*, that is an anomalous second peak in the magnetization loops. The origin of the second peak line $H_{sp}(T)$ is controversial, and has been attributed to mechanisms varying from dimensional crossover [7], collective pinning [8], crossover between different pinning phases, crossover to a disordered vortex glass [9–11], etc.

Only recently the vortex lattice (VL) has been directly observed in overdoped LSCO by means of small angle neutron scattering (SANS), revealing a field-induced transition from hexagonal to square symmetry [12,13] and the vanishing of the VL signal at temperatures well below T_{c2} [14]. In the underdoped regime of LSCO, on the other hand, a more disordered vortex glass has been observed by means of muon spin rotation (μSR) experiments [15]. Interestingly, recent inelastic neutron scattering (INS) experiments indicate a possible interplay

[a] *Present address:* Bruker BioSpin AG, 8117 Fällanden, Switzerland
e-mail: gilardi@hispeed.ch

between the vortex and copper-spin degrees of freedom. In optimally doped LSCO, sub-gap spin excitations induced by a magnetic field of 7.5 Tesla have been observed at low-temperatures [16]. Moreover, the spin gap was found to close at the irreversibility temperature rather than at T_{c2} [16,17]. In underdoped LSCO, field-induced static incommensurate magnetic peaks have been observed [18], and it has been suggested that these field-induced magnetic signals arise from antiferromagnetic order in the vortex cores and in the surrounding regions [19–21]. Enhanced antiferromagnetic spin correlations in the vortex core region have been indeed observed in NMR experiments [22,23].

In order to understand these experiments performed in the presence of an external magnetic field, it is crucial to have a good knowledge of the rich and complicated magnetic phase diagram of HTSC. We will present here a detailed study of the doping dependence of the magnetic phase diagram in LSCO single crystals from a macroscopic point of view.

2 Experimental

The magnetic phase diagram of LSCO has been investigated by means of magnetization (M) and ac-susceptibility (χ) measurements. We used a quantum design physical properties measurements system (PPMS) up to fields of 8 T applied approximately perpendicular to the CuO_2 planes. The angle Θ between the field direction and the c-axis of the samples was always smaller than 10 degrees. This precision is good enough for the present study, since the critical lines (e.g. melting line H_m, upper critical field H_{c2}) are known to be only slightly affected by small Θ angles (e.g. $H_m(\Theta) \sim H_m(\Theta = 0)/\cos(\Theta)$, $H_{c2}(\Theta) \sim H_{c2}(\Theta = 0)/\cos(\Theta)$)[24,25].

Four high quality LSCO single crystals with different doping levels have been measured. Details of the sample growth can be found elsewhere [26]. The samples are labeled by the doping region (OD for overdoped and UD for underdoped) together with their T_c, defined by $\chi'(T_c) = \frac{1}{2}\chi'(0\ \mathrm{K})$. The width of the superconducting transition ΔT_c has been determined by the 10%–90% criterion. OD-31K is a highly overdoped ($x = 0.20$, $T_c = 31.5$ K, $\Delta T_c = 2.8$ K) 51 mg crystal. OD-36K is slightly overdoped ($x = 0.17$, $T_c = 36.2$ K, $\Delta T_c = 1.5$ K) and is a portion of the crystal used for our SANS and INS experiments [12,17]. While most of the measurements on the OD-36K sample have been performed on a 293 mg cylindrical crystal, for zero-field cooled magnetization measurements the crystal has been cut to a 84 mg plate-like shape with the c-axis parallel to the largest face, in order to reduce the diamagnetic signal. UD-29K is an underdoped ($x = 0.10$, $T_c = 29.2$ K, $\Delta T_c = 1.3$ K) 37 mg plate-like crystal with the c-axis parallel to the largest face, which has been cut from a larger crystal used in μSR experiments [15]. Finally, UD-19K is a highly underdoped ($x = 0.075$, $T_c = 19$ K, $\Delta T_c = 3.8$ K) 52 mg plate-like crystal with the c-axis perpendicular to the largest face.

3 Results

We start with the complex ac-susceptibility $\chi = \chi' + \mathrm{i}\chi''$. The samples are placed in an external magnetic field $H_{ext} = H_{dc} + H_{ac} \cdot \cos(\omega_{ac} t)$, with $H_{ac} = 10$ Oe and $\omega_{ac} = 10$ Hz, $0\ \mathrm{T} \leq H_{dc} \leq 8$ T. A set of field-cooled (FC) temperature scans $\chi(T)$ for the four LSCO samples in different magnetic fields is shown in Figure 1, with the real part χ' and imaginary part χ'' plotted separately. In all samples the peak in χ'' shifts toward low temperatures and sharpens with increasing magnetic field. However, the magnitude of the shift is strongly doping dependent: for UD-19K a magnetic field of 6 T is sufficient to shift the peak by $0.85T_c$, whereas for OD-31K the shift caused by a field of 8 T is only $0.45T_c$. The detailed field dependence will be discussed in Section 4. In Figure 2 a representative curve $\chi(T)$ measured at $H_{dc} = 3$T for UD-29K is plotted together with magnetization curves $M(T)$. One can notice that there is no difference between the zero-field cooled (ZFC) and the FC $\chi(T)$ data, whereas FC and ZFC $M(T)$ curves separate below the irreversibility temperature T_{irr}. Slightly above T_{irr} there is a jump in the magnetization, indicating the presence of a first order transition (FOT) [1,2]. Similar data have been obtained for the other samples and for other values of H_{dc}. The jump is more pronounced at high magnetic fields, and in UD-19K only a broad anomaly could be observed (to note is that in this sample the loss peaks in $\chi''(T)$ are very broad, as well).

The experimental T_{irr} is often obtained from the loss peak in $\chi''(T)$, which is directly related to the maximum slope in $\chi'(T)$ [27]. However, in our case, T_{irr} obtained by ac-susceptibility measurements is slightly higher than the "real" T_{irr}, and is concomitant to the jump in $M(T)$ at T_{FOT}. The irreversibility line and the FOT line are found to be close to each other in all the samples, and are therefore strongly related to each other. In the following we will consider only the FOT line in the phase diagram.

$M(T)$ data provide additional information about the vortex behavior. In the reversible region above T_{irr} a clear diamagnetic signal is present up to temperatures larger than T_c. This region is characterized by strong fluctuations and there is no well defined upper critical temperature T_{c2}. The temperature T_{fluct}, at which diamagnetic (superconducting) fluctuations appear, has been defined as the temperature where the data begin to deviate from the horizontal normal state line (see Fig. 2c). The simplest way to estimate T_{c2} is to use the extrapolation method based on the linear Abrikosov formula [28]. The transition temperature T_{c2} is derived from the intersection of a linear fit with the normal-state horizontal line, as shown in Fig. 2c. It was shown that this procedure is not totally correct for HTSC, where the Abrikosov linear region is limited to a small temperature range because of the rounding close to T_{c2} [29,30]. Indeed in the underdoped regime, where fluctuations are larger, using extrapolation we get unphysical values for the upper critical field (positive slope of $H_{c2}(T)$, see Sect. 4). However, treating the data as proposed by Landau and Ott [30] one gets more reasonable upper critical lines for all the samples (see Fig. 4).

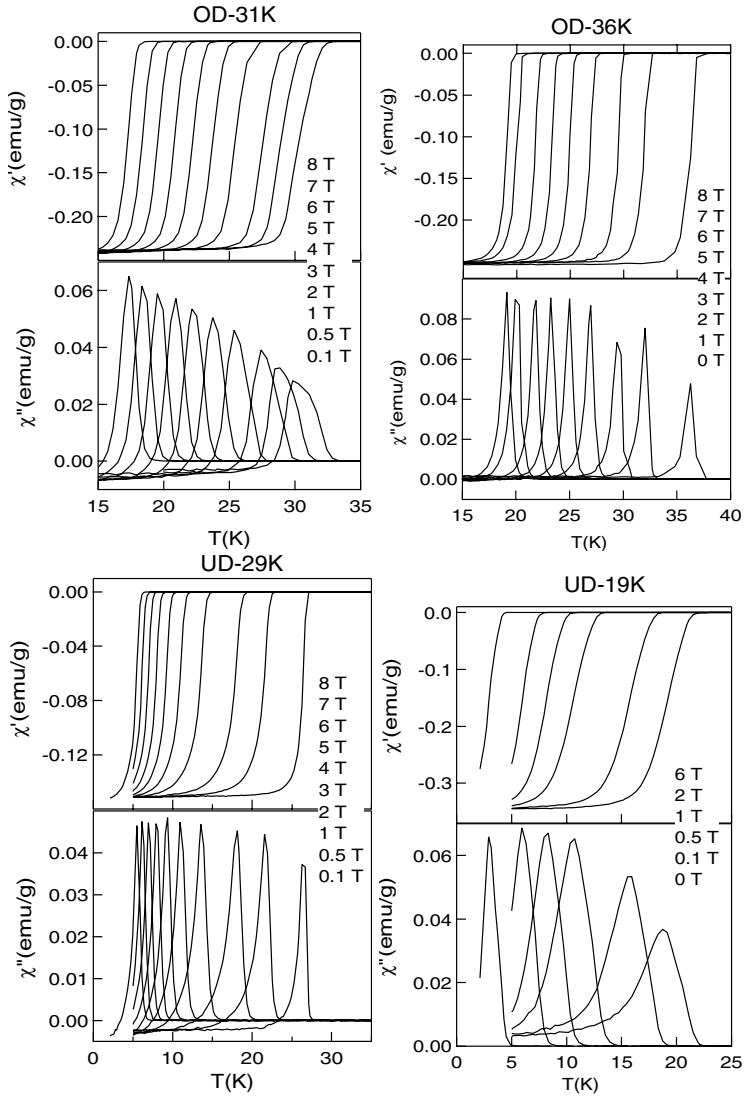

Fig. 1. Real and imaginary part of the ac-susceptibility $\chi(T)$ for OD-31K, OD-36K, UD-29K and UD-19K measured at different magnetic fields between 0 T and 8 T. The peak in $\chi''(T)$ rapidly shifts toward lower temperatures with increasing field.

We also performed isothermic ZFC $M(H)$ measurements at different temperatures (see Fig. 3). In the OD samples we could observe two peaks in the $M(H)$ curves (see Fig. 3a for OD-31K). The first minima H_p in the OD samples is known to be related to surface [31] and/or geometrical [32] barriers. Due to these barriers the field doesn't penetrate the bulk at the lower critical field H_{c1} but only at an higher field H_p. The second (and largest) minima H_{sp} (second peak) is related to some flux-pinning mechanism, although its origin is controversial [7–10]. In UD samples only one peak could be observed. We argue that this is actually the second peak H_{sp}. The penetration field H_p is most probably hidden, due to the low value of H_{sp}. This interpretation is supported by the fact that even in the OD samples it is difficult to identify H_p at high temperatures close to T_c (where H_{sp} occurs at low fields). Moreover, very accurate SQUID measurements on UD-29K clearly showed the presence of two minima at H_p and H_{sp} even in the underdoped regime [15]. We also performed some full hysteresis loops, as shown in the insets of Figure 3. The ascending and the descending branches meet at H_{irr}, whose values are consistent with those obtained by FC-ZFC $M(T)$ curves.

In order to facilitate the analysis and discussion of the experimental results, the characteristic fields ($H_{c2}(T)$, $H_{fluct}(T)$, $H_{FOT}(T)$ and $H_{sp}(T)$) of the four samples have been plotted in the H *vs* T phase diagrams shown in Figure 4. The magnetic phase diagram of LSCO is usually divided in four main phases:

1. Above the upper critical field $H_{c2}(T)$, LSCO is in the non-superconducting state and the magnetic flux is free to enter the crystal homogeneously.
2. Between $H_{c2}(T)$ and $H_{FOT}(T)$ ($H_{irr}(T)$) the magnetic flux is partially expelled from the superconductor. The magnetic field is present in the sample in the form of vortices which are in a reversible regime. In this region the vortices are thermally activated and highly dynamic.

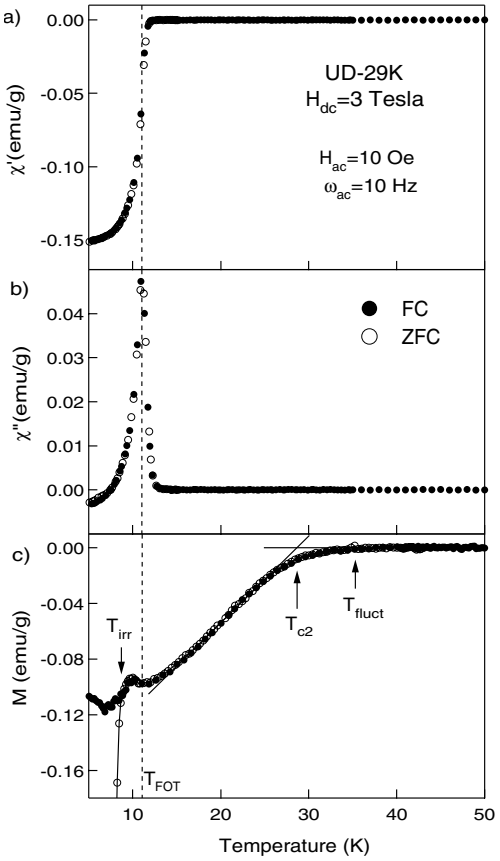

Fig. 2. a) Real and b) imaginary part of the ac-susceptibility $\chi(T)$ of UD-29K in an external field of 3 T. T_{FOT} is determined by the peak position in $\chi''(T)$, which corresponds to the maximum slope in $\chi'(T)$. c) Magnetization data measured at $H_{dc} = 3$ T, after subtraction of a linear background taken in the normal state. Below T_{irr} the FC and ZFC $M(T)$ curves separate, whereas at T_{FOT} a jump is observed. T_{c2} is estimated by extrapolation (see text). T_{fluct} is defined as the temperature where the data deviates from the horizontal normal state line.

3. Below $H_{FOT}(T)$ ($H_{irr}(T)$) the vortices are in an irreversible regime, as can be seen by the difference in the FC/ZFC data or in the hysteresis loops. Here the vortices are frozen in a lattice (VL), which can be directly observed in SANS experiments [12–14].
4. Below $H_p(T)$ (ideally $H_{c1}(T)$) the system is in the Meissner state and the flux is completely expelled from the bulk of the sample.

Indeed we can roughly understand our results in LSCO within this description, even though we have some additional lines in the phase diagram (e.g. H_{sp} and H_{fluct}). The first observation is that the magnetic phase diagrams of OD and UD LSCO are *qualitatively* similar but *quantitatively* very different. In particular for the UD samples the reversible region is much larger than for OD ones, whereas the second peak line occurs at much lower fields.

Table 1. Characteristic parameters for LSCO as a function of the Sr concentration x. The values of the upper critical field $H_{c2}(0\text{ K})$ [6], of the penetration depth λ_{ab} [37], and of the anisotropy γ [2,44,38] have been extrapolated from experimental values found in the literature. H_m and m have been obtained by fitting the data by equation (1), the Lindemann number c_L using equation (2). γ_{subl} and γ_{dec} are the anisotropies obtained by fitting our data using the sublimation, respectively decoupling models. Finally, the exponent n has been obtained by fitting the data with equation (5).

LSCO	OD-31K	OD-36K	UD-29K	UD-19K
x	0.20	0.17	0.10	0.075
T_c	31.5 K	36.2 K	29.2 K	19 K
ΔT_c	2.8 K	1.5 K	1.3 K	3.8 K
$H_{c2}(0\text{ K})$	∼45 T	∼60 T	∼45 T	∼35 T
λ_{ab}	1970 Å	∼2400 Å	2800 Å	∼3000 Å
γ	20(2)	20(2)	45(5)	60(5)
H_m	30 T	28 T	15 T	15 T
m	1.7	1.8	3.3	6.1
c_L	0.28	0.29	0.20	0.16
γ_{subl}	20	22	47	64
γ_{dec}	12	13	40	85
n	2.3	2.1	2.1	2.5

4 Discussion

Before discussing the possible reasons for this strong doping dependence of the phase diagram we want to have a detailed look at the single lines.

We start from the upper critical line $H_{c2}(T)$, which is not well defined since fluctuations are very strong near T_{c2}. This is more pronounced in the underdoped regime, where diamagnetic fluctuations are present even at temperatures T_{fluct} much larger than T_c. This anomalous behavior in the underdoped regime has also been observed in Nernst [33–35] and scanning SQUID microscopy [36] experiments and has been interpreted as being due to vortex-like excitations in the pseudogap region. As a consequence, $H_{c2}(T)$ as determined by extrapolation has an unphysical positive slope. In order to get more reasonable upper critical field lines, we used the Landau-Ott scaling procedure for magnetization data [30], taking the values of $H_{c2}(0\text{ K})$ listed in Table 1. The resulting $H_{c2}(T)$ lines are plotted in Figure 4.

We turn now to the FOT line $H_{FOT}(T)$, which is usually identified with the melting line [3–5], that is the transition of the vortex-solid into a vortex-liquid, in which the VL loses its shear modulus. The temperature dependence of $H_{FOT}(T)$ is predicted by the melting theory to be [3–5]:

$$H_{melt}(T) = H_m \cdot \left(1 - \frac{T}{T_c}\right)^m. \qquad (1)$$

The prefactor is known to depend almost only on the anisotropy of the system. In fact, considering $H_m \sim \gamma^{-2} T_c^{-2} \lambda_{ab}^{-4}$ (λ_{ab} is the in-plane penetration depth) and the fact that $T_c^{-2}\lambda_{ab}^{-4}$ is almost constant [39], one obtains $H_m \sim \gamma^{-2}$. Fitting our data by this model is not satisfactory, since we obtain a huge doping dependence of the

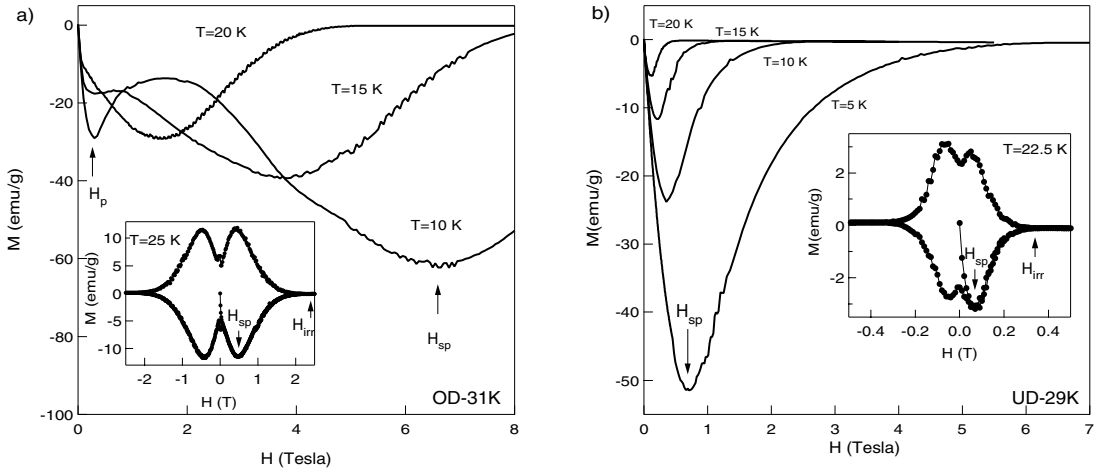

Fig. 3. ZFC isothermic magnetization curves for a) OD-31K and b) UD-29K. For OD-31K, H_p and H_{sp} have been determined as indicated by the arrows. For UD-29K, only H_{sp} could be observed. The insets show full hysteresis loops with H_{irr}.

exponent m and the prefactor H_m doesn't follow the expected γ dependence (see Tab. 1). Moreover, in all SANS experiments on HTSC [13,40,41] the ring-like intensity expected between H_{FOT} and H_{c2} for a liquid of *straight* vortices [42] has never been observed. A more precise melting theory, still based on the Lindemann criterion [43], predicts a more complicated temperature dependence of the melting line [3]:

$$H_{melt}(T) = \frac{4c_L^4 H_{c2}(0)\frac{B}{G}(\frac{T_c}{T}-1)^2}{\left(1+\sqrt{1+4c_L^4\frac{B}{G}(\frac{T_c}{T}-1)\frac{T_c}{T}}\right)^2} \qquad (2)$$

where $G = \frac{1}{2}(\frac{\gamma k_B T_c}{(4\pi/\mu_0)H_c^2(0)\xi_{ab}^3(0)})^2$ is the Ginzburg number (μ_0 is the permeability of free space, k_B is the Boltzmann's constant, H_c is the thermodynamic critical field, and ξ_{ab} is the in-plane coherence length), $B \approx 5.6$ and c_L is the Lindemann number. However, even this formula doesn't describe our data very well, since the fitted curves are unsatisfactory (see for example Fig. 4c for UD-29K), c_L is doping dependent and in some cases higher than the expected values ($c_L \sim 0.1$–0.2).

An alternative model to the melting transition is given by the sublimation theory [1,2], based on the strong anisotropy originating from the layered structure intrinsic to all HTSC. Within this scenario the melting is accompanied by the simultaneous decoupling of the vortex lines into 2D pancake vortices (*vortex gas*). The phenomenological scaling law which applies to all HTSC has been introduced by Sasagawa et al. and is given by [1,2]:

$$H_{subl}(T)[Oe] = 2.85 \cdot \gamma^{-2} s^{-1}\left(\frac{T_c}{T}-1\right) \qquad (3)$$

where s is the distance between the CuO_2 layers (6.6×10^{-8} cm in LSCO). This formula has been used in order to explain the FOT transition in many HTSC and nicely fits our data. γ is the only free parameter, and the fitted values are in good agreement with the measured values of the anisotropy (see Tab. 1). Our results in LSCO are of particular interest, because they extend the experimental data from a relatively narrow doping range ($0.09 \leq x \leq 0.15$[1,2]) to the very underdoped ($x = 0.075$) and overdoped ($x = 0.20$) regimes. Our observations show that equation (3) holds over a very large doping range in LSCO, and strongly support the sublimation scenario.

It remains to discuss the second peak line $H_{sp}(T)$ which has been explained on the basis of the thermal decoupling theory [45–47], which predicts the suppression of long-range order in the direction of the applied field due to thermal fluctuations. The expected temperature dependence is [46]

$$H_{dec}(T) = H^* \cdot \left(\frac{T_c}{T}-1\right) \qquad (4)$$

with $H^* = \Phi_0^3/(16\pi^3 e k_B \mu_0 s \gamma^2 T_c \lambda_{ab}(0)^2)$, where Φ_0 is the flux quantum and $e \approx 2.718$ is the exponential number. This function doesn't fit well our data, as shown in Figure 4b for OD-36K. Moreover, the estimated values for γ, obtained by substituting the known values of s, T_c and $\lambda_{ab}(0)$ in the theoretical expression for B^*, are not satisfactory compared to the experimental values (see Tab. 1). Moreover recent SANS measurements [13] indicate that the diffraction signal from the vortex lattice persists up to $H_{FOT}(T)$ and therefore discredit decoupling occurring at the second peak line. It has been often suggested that the second peak is related to the transition to a more disordered *vortex glass* phase [9,10], and very recent experimental results confirm this interpretation [11,15]. Our experimental data are better fitted by a power law [48]

$$H_{sp}(T) = H_0 \cdot \left(1-\frac{T}{T_c}\right)^n \qquad (5)$$

as can be seen in Figures 4 and 5. The value of the exponent is close to $n = 2$ in all samples (see Fig. 5 and Tab. 1). Interestingly, the value of H_0 seems to be proportional to

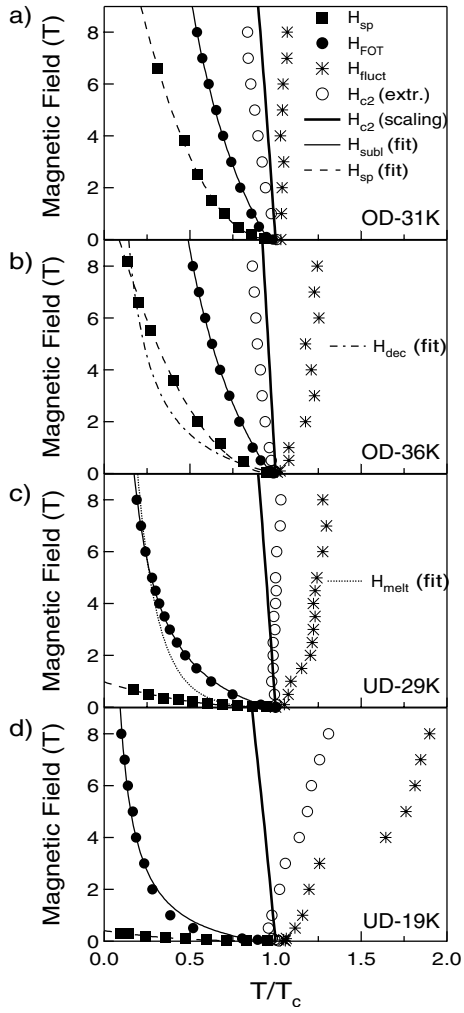

Fig. 4. Magnetic phase diagram of the four LSCO samples (OD-31K, OD-36K, UD-29K, UD-19K) showing the temperature dependencies of the second peak field $H_{sp}(T)$, the FOT line $H_{FOT}(T)$, the upper critical field $H_{c2}(T)$ (determined by extrapolation and by the scaling procedure), and the field $H_{fluct}(T)$ where diamagnetic fluctuations set in. In a)–d) the second peak line has been fitted by the power law (Eq. (5)), whereas the FOT line has been fitted by the sublimation model (Eq. (3)). In b) we have attempted to fit the second peak line by the decoupling theory (Eq. (4)), while in c) a fit of the FOT to the melting theory (Eq. (2)) is also shown.

γ^{-3}, even though (up to our knowledge) no theory predicts such a γ dependence. However, a large anisotropy naturally renders the vortex system more susceptible to disorder. The observed anisotropy dependence of $H_{sp}(T)$ is therefore in qualitative agreement with a scenario where the second peak line is related to a field-induced vortex glass transition.

5 Conclusion

A first look at the magnetic phase diagrams shown in Figure 4 could indicate that the vortex matter in LSCO is strongly doping dependent. This is true from a quantitative point of view, but qualitatively all samples display the same transitions (second peak, irreversibility, FOT and upper critical lines). The quantitative doping dependence of the magnetic phase diagram can mainly be explained by the different degree of anisotropy: H_{sp} is found to be proportional to γ^{-3} and H_{FOT} to γ^{-2}. The interpretation of the second peak in LSCO is still controversial but our data seem to favor the vortex glass scenario, whereas the FOT line is consistent to the sublimation theory rather than to the melting theory. Moreover, strong superconducting fluctuations above T_c have been observe in the underdoped regime.

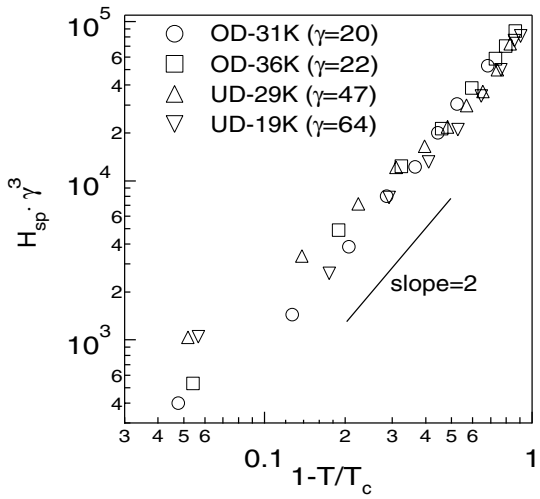

Fig. 5. Temperature dependence of $H_{sp} \cdot \gamma^3$ plotted in a double logarithmic scale. All the data measured in samples with different doping levels collapse on one line with slope ∼2. This indicates that the power law (Eq. (5)) has an exponent $n \approx 2$ and $H_0 \propto \gamma^{-3}$. We have used the values of γ obtained by fitting our data using equation(3) (γ_{subl} in Tab. 1).

We would like to thank C.D. Dewhurst for valuable discussions. This work was performed at the Paul Scherrer Institute, Switzerland, and was supported by the Swiss National Science Foundation and the Ministry of Education, Technology and Science of Japan (NM, MO).

References

1. T. Sasagawa, K. Kishio, Y. Togawa, J. Shimoyama, K. Kitazawa, Phys. Rev. Lett. **80**, 4297 (1998)
2. T. Sasagawa, Y. Togawa, J. Shimoyama, A. Kapitulnik, K. Kitazawa, K. Kishio, Phys. Rev. B **61**, 1610 (2000)
3. For a review, see G. Blatter, M.V. Feigelman, V.B. Geshkenbein, A.I. Larkin, V.M. Vinokur, Rev. Mod. Phys. **66**, 1125 (1994)
4. E.H. Brandt, Phys. Rev. Lett. **63**, 1106 (1989)
5. A. Houghton, R.A. Pelcovits, A. Sudbo, Phys. Rev. B **40**, 6763 (1989)
6. Y. Ando, G.S. Boebinger, A. Passner, L.F. Schneemeyer, T. Kimura, M. Okuya, S. Watauchi, J. Shimoyama, K. Kishio, K. Tamasaku, N. Ichikawa, S. Uchida, Phys. Rev. B **60**, 12475 (1999)

7. T. Tamegai, Y. Iye, I. Oguro, K. Kishio, Physica C **213**, 33 (1993)
8. L. Krusin-Elbaum, L. Civale, V.M. Vinokur, F. Holtzberg, Phys. Rev. Lett. **69**, 2280(1992)
9. T. Giamarchi, P. Le Doussal, Phys. Rev. B **55**, 6577 (1997)
10. A.E. Koshelev, V.M. Vinokur, Phys. Rev. B **57**, 8026 (1998)
11. D. Giller, A. Shaulov, R. Prozorov, Y. Abulafia, Y. Wolfus, L. Burlachkov, Y. Yeshurun, E. Zeldov, V.M. Vinokur, J.L. Peng, R.L. Greene, Phys. Rev. Lett. **79**, 2542 (1997)
12. R. Gilardi, J. Mesot, A. Drew, U. Divakar, S.L. Lee, E.M. Forgan, O. Zaharko, K. Conder, V.K. Aswal, C.D. Dewhurst, R. Cubitt, N. Momono, M. Oda, Phys. Rev. Lett. **88**, 217003 (2002)
13. R. Gilardi, J. Mesot, A.J. Drew, U. Divakar, S.L. Lee, N.H. Andersen, J. Kohlbrecher, N. Momono, M. Oda, Physica C **408-410**, 491 (2004)
14. R. Gilardi, S. Streule, J. Mesot, A.J. Drew, U. Divakar, S.L. Lee, S.P. Brown, E.M. Forgan, N. Momono, M. Oda, Int. J. Mod. Phys. B **17**, 3411 (2003)
15. U. Divakar, A.J. Drew, S.L. Lee, R. Gilardi, J. Mesot, F.Y. Ogrin, D. Charalambous, E.M. Forgan, G.I. Menon, N. Momono, M. Oda, C.D. Dewhurst, C. Baines, Phys. Rev. Lett. **92**, 237004 (2004)
16. B. Lake, G. Aeppli, K.N. Clausen, D.F. McMorrow, K. Lefmann, N.E. Hussey, N. Mangkorntong, M. Nohara, H. Takagi, T.E. Mason, A. Schrder, Science **291**, 1759 (2001)
17. R. Gilardi, A. Hiess, N. Momono, M. Oda, M. Ido, J. Mesot, Europhys. Lett. **66**, 840 (2004)
18. B. Lake, H.M. Rønnow, N.B. Christensen, G. Aeppli, K. Lefmann, D.F. McMorrow, P. Vorderwisch, P. Smeibidl, N. Mangkorntong, T. Sasagawa, M. Nohara, H. Takagi, T.E. Mason, Nature **415**, 299 (2002)
19. D.P. Arovas, A.J. Berlinsky, C. Kallin, S.-C. Zhang, Phys. Rev. Lett. **79**, 2871 (1997)
20. E. Demler, S. Sachdev, Y. Zhang, Phys. Rev. Lett. **87**, 067202 (2001)
21. J.P. Hu, S.-C. Yhang et al., J. Phys. Chem. Sol. **63**, 2277 (2002)
22. V.F. Mitrovic, E.E. Sigmund, M. Eschrig, H.N. Bachman, W.P. Halperin, A.P. Reyes, P. Kuhns, W.G. Moulton, Nature **413**, 501 (2001)
23. K. Kakuyanagi, K. Kumagai, Y. Matsuda, M. Hasegawa, Phys. Rev. Lett. **90**, 197003 (2003)
24. U. Welp, W.K. Kwok, G.W. Crabtree, K.G. Vandervoort, J.Z. Liu, Phys. Rev. B **40**, R5263 (1989)
25. A. Schilling, U. Welp, W.K. Kwok, G.W. Crabtree, Phys. Rev. B **65**, 054505 (2002)
26. The TSFZ-method was used for the crystal growth, see e.g. T. Nakano, N. Momono, M. Oda, M. Ido, J. Phys. Soc. Jpn. **67**, 2622 (1998)
27. F. Gömöry, Supercond. Sci. Technol. **10**, 523 (1997)
28. A.A. Abrikosov, Zh. Eksp. Teor. Fiz. **32**, 1442 (1957)
29. Z. Hao, J.R. Clem, M.W. McElfresh, L. Civale, A.P. Malozemoff, F. Holtzberg, Phys. Rev. B **43**, 2844 (1991)
30. I.L. Landau, H.R. Ott, Phys. Rev. B **66**, 144506 (2002)
31. L. Burlachkov, V.B. Geshkenbein, A.E. Koshelev, A.I. Larkin, V.M. Vinokur, Phys. Rev. B **50**, R16770 (1994)
32. E. Zeldov, A.I. Larkin, V.B. Geshkenbein, M. Konczykovski, D. Majer, B. Khaykovich, V.M. Vinokur, H. Shtrikman, Phys. Rev. Lett. **73**, 1428 (1994)
33. Y. Wang, N.P. Ong, Z.A. Xu, T. Kakeshita, S. Uchida, D.A. Bonn, R. Liang, W.N. Hardy, Phys. Rev. Lett. **88**, 257003 (2002)
34. Z.A. Xu, N.P. Ong, Y. Wang, T. Kakeshita, S. Uchida, Nature **406**, 486 (2001)
35. H.H. Wen, Z.Y. Liu, Z.A. Xu, Z.Y. Weng, F. Zhou, Z.X. Zhao, Europhys. Lett. **63**, 583 (2004)
36. I. Iguchi, T. Yamaguchi, A. Sugimoto, Nature **412**, 420 (2001)
37. C. Panagopoulos, B.D. Rainford, J.R. Cooper, W. Lo, J.L. Tallon, J.W. Loram, J. Betouras, Y.S. Wang, C.W. Chu, Phys. Rev. B **60**, 14617 (1999)
38. M. Willemin, C. Rossel, J. Hofer, H. Keller, A. Revcolevschi, Phys. Rev. B **59**, R717 (1999)
39. This assumption has been established by μSR studies which show that T_c is proportional to the muon-spin relaxation rate $\sigma \sim \lambda^{-2}(0)$ in any compound, see e.g. Y.J. Uemura et al., Phys. Rev. Lett. **62**, 2317 (1989); Y.J. Uemura et al., Phys. Rev. Lett. **66**, 2665 (1991)
40. R. Cubitt, E.M. Forgan, G. Yang, S.L. Lee, D. McK. Paul, H.A. Mook, M. Yethiraj, P.H. Kes, T.W. Li, A.A. Menovsky, Z. Tarnawski, K. Mortensen, Nature **365**, 407 (1993)
41. C.M. Aegerter, S.T. Johnson, W.J. Nuttall, S.H. Lloyd, M.T. Wylie, M.P. Nutley, E.M. Forgan, R. Cubitt, S.L. Lee, D. McK. Paul, M. Yethiraj, H.A. Mook, Phys. Rev. B **57**, 14511 (1998)
42. H. Nordborg, G. Blatter, Phys. Rev. Lett. **79**, 1925 (1997)
43. F. Lindemann, Phys. Z. **11**, 69 (1910)
44. T. Kimura, K. Kishio, T. Kobayashi, Y. Nakayama, N. Motohira, K. Kitazawa, K. Yamafuji, Physica C **192**, 247 (1992)
45. L.I. Glazman, A.E. Koshelev, Phys. Rev. B **43**, 2835 (1991)
46. L.L. Daemen, L.N. Bulaevskii, M.P. Maley, J.Y. Coulter, Phys. Rev. Lett. **70**, 1167 (1993)
47. I.M. Sutjahja, A.A. Nugroho, M.O. Tjia, A.A. Menovsky, J.J.M. Franse, Phys. Rev. B **64**, 134502 (2001)
48. Y. Kodama, K. Oka, Y. Yamaguchi, Y. Nishihara, K. Kajimura, Phys. Rev. B **56**, 6265 (1997)